68th International Astronautical Congress, Adelaide, Australia.

IAC-17,C1,1,2,x38510

Force and Torque Disturbance Modeling Due to General Thruster Plume Impingements

Thibaud Teil[a] and Hanspeter Schaub[b]

[a] *Graduate Research Assistant, Department of Aerospace Engineering Sciences, University of Colorado, 431 UCB, Colorado Center for Astrodynamics Research, Boulder, CO 80309-0431.*, hanspeter.schaub@colorado.edu

[b] *Professor, Glenn L. Murphy Chair of Engineering, Department of Aerospace Engineering Sciences, University of Colorado, 431 UCB, Colorado Center for Astrodynamics Research, Boulder, CO 80309-0431.*, hanspeter.schaub@colorado.edu

Abstract

Thruster plumes can intercept neighboring surfaces on the host spacecraft which can lead to unwanted disturbance and heating effects. The placement and direction of the thrusters relative to surfaces of concern, such as solar arrays, is either done intuitively or with intensive computational fluid methods. The methodology presented evaluates forces and torques from thruster plume impingement on the spacecraft surfaces. This becomes a modular tool for spacecraft design. Due to its speed of evaluating the full impingement it allows for real-time attitude and navigation simulations even if the structures are time varying. This plume impingement study therefore allows for objective thruster placement, and higher fidelity simulations in support of future attitude control designs, allowing for more stringent pointing requirements. This paper applies a general mathematical derivation of conical intersections to the plume impingement problem. The simulations presented allow for the study of any number of thrusters with a surface of arbitrary orientation. Using the derived conical functions to bound the region where the plume is acting, the pressure profile is integrated yielding forces and torques. In order to maintain a modular, reusable code, the pressure function from the thruster is applied independently instead of being modeled analytically. This novel and modular approach allows precise thruster impingement effects to be considered in faster-than-realtime numerical analysis.

1. Introduction

As spacecraft geometries become more compact and mobile, the question of thruster placement and its consequences on disturbance forces and torques is amplified. Spacecraft design requirements regarding the location of power generation, sensor and communication structures can lead to unwanted, temporary thruster plume impingements. Although Computational Fluid Dynamics (CFD) studies provide accurate perturbation forces and torques [1], as well as thermal analysis on the surfaces [2, 3], it is a computationally costly analysis and unsuitable for faster-than-realtime numerical analysis. Furthermore, as flexible, deployable, and mobile surfaces become more common, it is desirable to have estimates of the perturbation forces and heating throughout the mission. Figure 1 presents a schematic of a plume impingement scenario where a thruster is directed towards a solar panel.

Reference 4 evaluates plume impingements for docking protocols for MIR and the Space Shuttle, while References 5 and 6 study the plume impingements for the International Space Station (ISS). Solar panels are indeed the most susceptible surface, and is the most common data source for thruster plume impingement [7]. When adding the challenge of mobile panels as seen on the ISS, having instantaneous feedback concerning plume impingement, with faster-than-realtime evaluations, is a valuable asset.

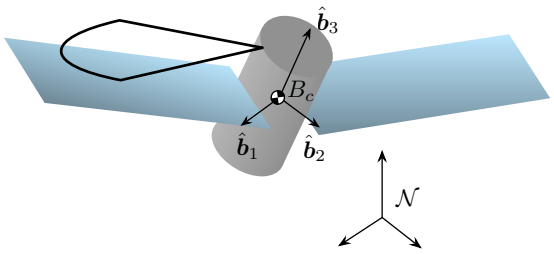

Fig. 1: Example of plume impingement on a solar panel

The goal of this paper is to develop a general force and torque model, given any thruster orientation, surface orientation, and any plume pressure function. A user will input a thruster and panel location and orientation, as well as a thruster pressure function to compute the forces and torques acting on the body as the thruster is ignited. Thus, this work assumes a good thruster plume model has already been created in prior work using CFD simulation or using experimental data. In the context of a static spacecraft, these forces and torques are computed once, and their values are used throughout the simulation. They can therefore be used as library values that are read instantaneously.

In the context of reconfigurable spacecrafts with time-varying geometries (such as the ISS), the goal is to allow for fast computation capabilities. This leads to the abil-

ity to compute disturbance forces and torques faster-than-realtime, yielding higher-fidelity simulations, and warnings of dangerous thruster and panel placements.

In order to do this, an analytical solution for the plume's intersection with the surface of concern is developed. This comes with the assumption that the plume is modeled by a cone with a fixed angle defined in the thruster's pressure function. The bounds are defined both by the conical intersection between the surface and the cone, and by the size of the panel. This paper uses rectangular panels of adjustable size, which corresponds to the flat plate nature of most spacecraft structures.

Different scenarios for thruster plume impingement are first categorized, followed by the development of the equation for the plume hyperbola. The remaining bounds are then made explicit as a result of this analytical function. Models of the different types of pressure functions are presented next, which leads to the integration method of the forces and torques. In the conclusion future work regarding heating issues is discussed.

2. Hyperbola characterization

2.1 Surface of interest

At any given instant, there can be different plume impingement geometries incident on a spacecraft structure. The intersection of an infinite plane and a cone produce three possible types of conical sections. In order to formulate the problem, it is first assumed that the surface of interest is an infinite plane, with one notable point on it: the center of the actual finite surface of interest.

2.1.1 Frames defined

The following frames are defined:

- The body frame of the spacecraft $\mathcal{B} : \{\hat{\boldsymbol{b}}_1, \hat{\boldsymbol{b}}_2, \hat{\boldsymbol{b}}_3\}$ is a frame fixed to the spacecraft structure, on the center of mass.
- The surface frame on the impinged panel $\mathcal{S} = \{\hat{\boldsymbol{u}}, \hat{\boldsymbol{v}}, \hat{\boldsymbol{w}}\}$. This frame is centered on the surface, and has $\hat{\boldsymbol{w}}$ as a normal unit vector to its surface. These parameters are illustrated in Figure 2.
- The thruster frame is $\mathcal{T} : \{\hat{\boldsymbol{t}}_1, \hat{\boldsymbol{t}}_2, \hat{\boldsymbol{t}}_3\}$. This frame is fixed relative to the thruster cone, with $\hat{\boldsymbol{t}}_2$ pointed in the thrust direction, and $\hat{\boldsymbol{t}}_1$ is towards the plane. This frame is visualized in Figure 3.
- The hyperbola frame is $\mathcal{C} = \{\hat{\boldsymbol{u}}_c, \hat{\boldsymbol{v}}_c, \hat{\boldsymbol{w}}_c = \hat{\boldsymbol{t}}_3\}$. This frame is centered on the hyperbola, and is illustrated in Figure 4.

2.1.2 Parameters defined

The study considers a single thruster that can impinge on a single panel:

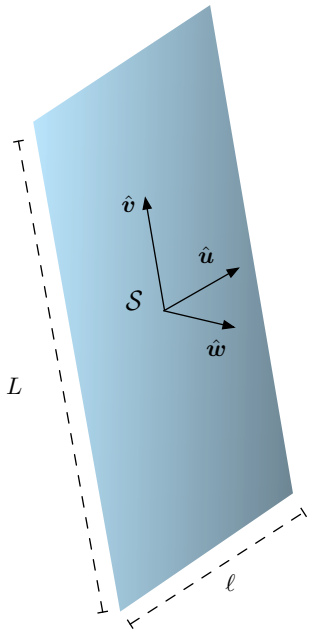

Fig. 2: $\mathcal{S}$ frame defined on surface of interest

- Thruster: Defined by a direction, position in the spacecraft body frame, and a pressure function.
- Panel: Defined by a normal unit vector $\hat{\boldsymbol{w}}$, a center position in the body frame, a length (L), and a width (ℓ).

2.1.3 Surface equations

The following geometrical definitions are easiest in the thruster frame. In the surface frame the vector $\hat{\boldsymbol{w}}$ is simple to express as

$$ {}^{\mathcal{S}}\hat{\boldsymbol{w}} = \begin{bmatrix} 0 \\ 0 \\ 1 \end{bmatrix}^{\mathcal{S}} \tag{1} $$

The left superscript notation labels with respect to what frame the vector components are taken [8]. The Direction Cosine Matrix (DCM) between two frames $\mathcal{B}$ and $\mathcal{N}$ is written as $[\mathcal{BN}]$. By computing the DCM between these two frames, the normal vector to our plane in $\mathcal{T}$ is

$$ {}^{\mathcal{T}}\hat{\boldsymbol{w}} = [\mathcal{TS}]^{\mathcal{S}}\hat{\boldsymbol{w}} = \begin{bmatrix} n \\ m \\ p \end{bmatrix}^{\mathcal{T}} \tag{2} $$

The unit vector $\hat{\boldsymbol{t}}_2$ is chosen along the cone axis, with an opening angle $\tan 2\alpha = c$. In the $\mathcal{T}$ frame, Eq. (3) represents the identity that must satisfy the points on a cone, where (x, y, z) are components in the $\{\hat{\boldsymbol{t}}_1, \hat{\boldsymbol{t}}_2, \hat{\boldsymbol{t}}_3\}$ frame.

$$ x^2 + z^2 = c^2 y^2 \tag{3} $$

The cone is assumed right, so the coefficients for x and z are normalized. The surface plane constraint equation

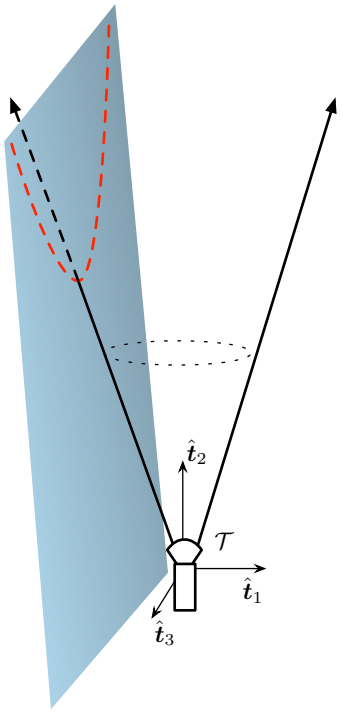

Fig. 3: A thruster centered in $\mathcal{T}$ has a plume cone which intersects the surface. The dotted red line represents the intersection of the cone and the plane.

with normalized n, m, p coefficients

$$n^2 + m^2 + p^2 = 1$$

is written as

$$\begin{aligned} & nx + my + pz = nx_0 + my_0 + pz_0 \\ \Rightarrow\ & nx + my + pz = d \end{aligned} \tag{4}$$

This plane is defined by point $\hat{\boldsymbol{w}}_0 = (x_0, y_0, z_0)^T$, and the coefficients of the normal unit vector $\hat{\boldsymbol{w}}$ given in Eq. 2. The scalar d represents the distance from the thruster frame origin to $\hat{\boldsymbol{w}}_0$.

Knowledge of the thruster plume location and orientation defines c, while knowledge of the spacecraft geometry fully defines m, n, p, d, as well as the DCMs needed to change frames.

2.1.4 Conical Section of Plume Impingement

The conical section is derived by substituting the plane equation into the cone equation, as all sets of coordinates in the $\mathcal{T}$ frame which are solutions to Eq. (3) and Eq. (4) represent points both on the plane, and on the cone. Coordinates which satisfy both of these constraint functions, will define the conical intersection:

$$x^2 + \left(\frac{d - nx - py}{m}\right)^2 = c^2 y^2 \tag{5}$$

$$\begin{aligned} \Rightarrow & \left(1 + \frac{n^2}{m^2}\right) x^2 + \frac{2np}{m^2} xy + \left(\frac{p^2}{m^2} - c^2\right) y^2 \\ & - \frac{2dn}{m^2} x + \frac{2d}{m^2} y + \frac{d^2}{m^2} = 0 \end{aligned} \tag{6}$$

$$\begin{aligned} \Rightarrow & A_{xx} x^2 + 2A_{xy} xy + A_{yy} y^2 + 2B_x x \\ & + 2B_y y + C = 0 \end{aligned} \tag{7}$$

Since the thrusters first axis (or x axis) is chosen to be pointing away from the plane, the m component doesn't go to zero unless the thruster is on the surface.

The conical discriminant is then defined:

$$\begin{aligned} \Delta = \begin{vmatrix} A_{xx} & A_{xy} \\ A_{xy} & A_{yy} \end{vmatrix} &= \begin{vmatrix} \left(1 + \frac{n^2}{m^2}\right) & \frac{np}{m^2} \\ \frac{np}{m^2} & \frac{p^2}{m^2} - c^2 \end{vmatrix} \\ &= \frac{p^2}{m^2} - c^2 \left(1 + \frac{n^2}{m^2}\right) \end{aligned} \tag{8}$$

The full system determinant:

$$\begin{aligned} \delta = \begin{vmatrix} A_{xx} & A_{xy} & B_x \\ A_{xy} & A_{yy} & B_y \\ B_x & B_y & C \end{vmatrix} &= \begin{vmatrix} 1 + \frac{n^2}{m^2} & \frac{np}{m^2} & -\frac{dn}{m^2} \\ \frac{np}{m^2} & \frac{p^2}{m^2} - c^2 & \frac{d}{m^2} \\ -\frac{dn}{m^2} & \frac{d}{m^2} & \frac{d^2}{m^2} \end{vmatrix} \\ &= \frac{d^2}{m^6} \left(m^2 p^2 - c^2 m^4 - m^2 - n^2 p^2 - 2n^2 p - n^2\right) \end{aligned} \tag{9}$$

The conical discriminant Δ determines the nature of the conical intersection [9].

- If $\Delta = \frac{p^2}{m^2} - c^2 \left(1 - \frac{n^2}{m^2}\right) > 0$, the intersection is an ellipse
- If $\Delta = \frac{p^2}{m^2} - c^2 \left(1 - \frac{n^2}{m^2}\right) < 0$, the intersection is a hyperbola
- If $\Delta = \frac{p^2}{m^2} - c^2 \left(1 - \frac{n^2}{m^2}\right) = 0$, the intersection is a parabola

Given the desired applications for this study, the use of hyperbolas was favored. The first assumption is hence that the thruster is aimed away from the surface, meaning that $(m^2 - n^2)c^2 > p^2$. This is revisited in the following sections. In order to simplify the formulation, the hyperbola is centered by applying Cramer's rule, thus zeroing

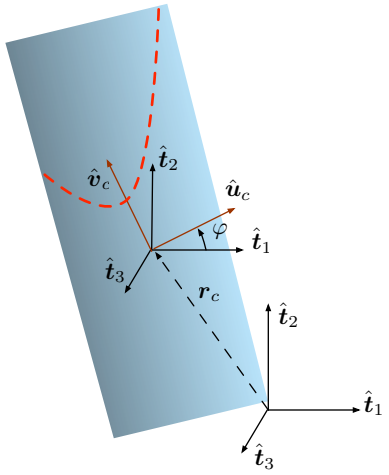

Fig. 4: Translation and Rotation from $\mathcal{T}$ to $\mathcal{C}$

the cross terms:

$$\begin{aligned} x_c &= -\frac{1}{\Delta}\begin{vmatrix} \frac{dn}{m^2} & \frac{np}{m^2} \\ \frac{d}{m^2} & \frac{p^2}{m^2} - c^2 \end{vmatrix} \\ &= -\frac{dn\left(c^2m^2 - p^2 + p\right)}{m^2\left(c^2\left(m^2+n^2\right) - p^2\right)} \end{aligned} \tag{10}$$

$$\begin{aligned} y_c &= -\frac{1}{\Delta}\begin{vmatrix} \frac{n^2}{m^2} + 1 & \frac{dn}{m^2} \\ \frac{np}{m^2} & \frac{d}{m^2} \end{vmatrix} \\ &= \frac{d\left(m^2 - n^2(p-1)\right)}{m^2\left(c^2\left(m^2+n^2\right) - p^2\right)} \end{aligned} \tag{11}$$

The equation can therefore be re-centered by defining $\bar{x} = x - x_c$ and $\bar{y} = y - y_c$, via a translation by vector $\boldsymbol{r}_c = {}^{\mathcal{T}}\begin{bmatrix} u_c & v_c \end{bmatrix}^T$ seen in Figure 4. The equation can be finally put in matrix form:

$$\begin{bmatrix} \bar{x} & \bar{y} \end{bmatrix} \underbrace{\begin{bmatrix} A_{xx} & A_{xy} \\ A_{xy} & A_{yy} \end{bmatrix}}_{[H]} \begin{bmatrix} \bar{x} \\ \bar{y} \end{bmatrix} + \frac{\delta}{\Delta} = 0 \tag{12}$$

where $[H]$ is a symmetric, square, real-valued matrix. It can therefore be diagonalized in an orthonormal frame, and the passage matrices are the DCMs that will rotate the frame to the adapted hyperbola frame. The eigenvalues λ_1 and λ_2 are given by the canonical quadratic equation:

$$\lambda^2 - \left(1 - c^2 + \frac{n^2+p^2}{m^2}\right)\lambda + \Delta = 0 \tag{13}$$

The eigenvectors define the 2-dimensional rotation matrix $[Q]$ such that: $[Q][\Lambda][Q]^T = [H]$. The $[Q]$ matrix has an associated rotation angle φ seen in Figure 4 and given by

$$\tan 2\varphi = \frac{2A_{xy}}{A_{xx} - A_{yy}} \tag{14}$$

Therefore the DCM from $\mathcal{T}$ to $\mathcal{C}$ is in equation (15).

$$[\mathcal{CT}] = \begin{bmatrix} Q & 0_{2\times 1} \\ 0_{1\times 2} & 1 \end{bmatrix} \tag{15}$$

This brings us into the centered frame $\mathcal{C} = (\hat{\boldsymbol{u}}_c, \hat{\boldsymbol{v}}_c, \hat{\boldsymbol{w}}_c = \hat{\boldsymbol{t}}_3)$, aligned with the surface, where the components are noted (u_h, v_h, z):

$${}^{\mathcal{C}}\begin{bmatrix} u_h \\ v_h \\ z \end{bmatrix} = [\mathcal{CT}] \, {}^{\mathcal{T}}\begin{bmatrix} x \\ y \\ z \end{bmatrix} \tag{16}$$

Because $\Delta = \lambda_1\lambda_2$, the hyperbola equation becomes

$$\begin{aligned} &\begin{bmatrix} u_h & v_h \end{bmatrix}\begin{bmatrix} \lambda_1 & 0 \\ 0 & \lambda_2 \end{bmatrix}\begin{bmatrix} u_h \\ v_h \end{bmatrix} + \frac{\delta}{\Delta} = 0 \\ \Rightarrow &-\frac{\lambda_1^2\lambda_2}{\delta}u_h^2 - \frac{\lambda_1\lambda_2^2}{\delta}v_h^2 = 1 \end{aligned} \tag{17}$$

The roots of Eq. (13), λ_1 and λ_2, give us the coefficients of the canonical form:

$$h_1^2 = -\frac{\delta}{\lambda_1^2\lambda_2} \tag{18}$$

$$h_2^2 = \frac{\delta}{\lambda_1\lambda_2^2} \tag{19}$$

yielding the canonical form for the hyperbola:

$$\frac{u_h^2}{h_1^2} - \frac{v_h^2}{h_2^2} = 1 \tag{20}$$

In this frame, the hyperbola is a bijection, and gives the lower bound of the intersection onto the frame with the function:

$$v_h = h(u_h) = \sqrt{h_2^2\left(\frac{u_h^2}{h_1^2} - 1\right)} \tag{21}$$

Hence, the points $\boldsymbol{c}$ on the conical, in the $\mathcal{C}$ frame are:

$$\forall u_h \in \mathbb{R}, {}^{\mathcal{C}}\boldsymbol{c} = {}^{\mathcal{C}}\begin{bmatrix} u_h \\ v_h = \sqrt{h_2^2\left(\frac{u_h^2}{h_1^2} - 1\right)} \\ \frac{1}{m}\left(d - nu_h - pv_h\right) \end{bmatrix} \tag{22}$$

2.2 Generalization

The general pressure function expression defining the thruster plume output is used to make this formulation applicable to any situation. If a thruster is placed in a way that leads to an ellipse (thruster pointed towards the panel), the pressure cone angle can be widened, by padding the pressure function with zeros. The new half angle cone is named $\tilde{\alpha}$ and defined in Eq. (23).

The angle between the thruster direction and the opposite of the panel normal is defined by $\theta = \arccos\left(\hat{\boldsymbol{\omega}} \cdot \hat{\boldsymbol{t}}_2\right)$.

$$\tilde{\alpha} = \alpha + \left(\frac{\pi}{2} - \theta - \alpha\right) + \eta \tag{23}$$

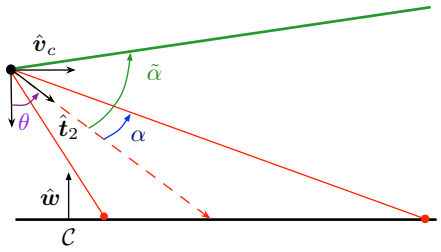

Fig. 5: Angles defined to widen the pressure cone

The η term is a margin term that pushes the cone angle above the 90° angle. It is chosen nominally to be 5° and avoids potential numerical issues with having a parabola for a conical intersection. This issue is illustrated in Figure 5.

This method always results in a hyperbola, and never compromises the pressure function, as it only pads it with zeros. This allows the method developed in this paper to be used in general scenarios. Even if the conical intersection is an ellipse, this padding method can bring it back to a hyperbola. This dramatically simplifies the study. It is noted that the hyperbola can also be inverted, a scenario that also exists if the pressure function is defined with a half-angle of more than 90°.

3. Surface bounds

3.1 Finding panel sides

In order to fully bound our integration, the next step reduces the infinite plane assumption to a bounded finite panel. This is done with knowledge of the hyperbola center, and the rotation $[Q]$ that rotated the $\hat{\boldsymbol{t}}_1$ and $\hat{\boldsymbol{t}}_2$ vectors by φ about $\hat{\boldsymbol{t}}_3$. The surface affected by the plume is delimited by the hyperbola equation that was found previously, and the edges of the finite panel. The equation of the edges of interest are known in the body frame $\mathcal{B}$, since the location and size of the panels are known. Hence in the body frame, every side is defined by a unit vector direction, and a point it crosses. This unit direction vector called $\hat{e}$:

The vector components are mapped to the $\mathcal{C}$ frame using

$$^{\mathcal{C}}\hat{\boldsymbol{e}} = [\mathcal{SC}]^T [\mathcal{BS}]^{T\,\mathcal{B}}\hat{\boldsymbol{e}} \tag{24}$$

Depending on whether this is a top edge or a side edge, two different points can be found lying on these bounding lines: Recall that the $\mathcal{S}$ frame is centered on the surface, and that the dimensions are L and ℓ for the length and width of the panel. There is no third vector component as it is constant and zero on the surface.

- If it is a top bound: $P = (\frac{\ell}{2}, \frac{L}{2} - v_c)$
- If it is a lateral bound: $P = (\frac{\ell}{2} - u_c, \frac{L}{2})$

Using the previous notation, P can be noted as $P = (p_u, p_v)$, and therefore each panel side has an equation written in (25), where the planar direction vector is $\hat{\boldsymbol{e}} = (a_{\mathcal{H}}, b_{\mathcal{H}})$ with it's coefficient defined in the $\mathcal{C}$ frame through the relationship

$$a_{\mathcal{H}}\,(u - p_u) + b_{\mathcal{H}}\,(v - p_v) = 0 \tag{25}$$

This is the general form of the panel edges, the associated vectors are illustrated in Figure 6.

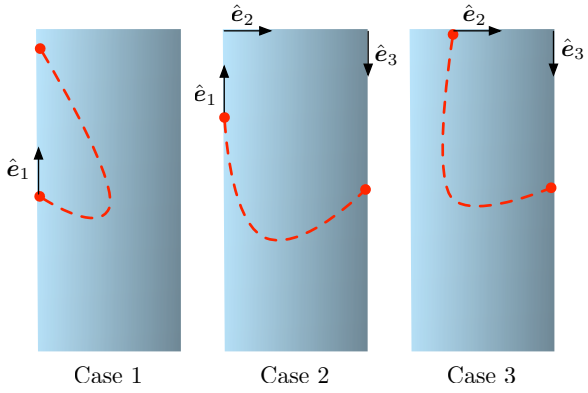

Fig. 6: Different impingement scenarios

3.2 Cases

This subsection consideres that the hyperbola center is on the finite surface of concern. The different possible integration geometries are summarized in Figure 6. These will define the points of interest.

- Case 1: Equating (20) with (25) yields two solutions for one of the panel side equations.
- Case 2: Equating (20) with (25) yields one solution for two of the panel side equations, which have a common point.
- Case 3: Equating (20) with (25) yields one solution for two of the panel side equations, which do not intersect.

These cases do not cover all the possible scenarios. The hyperbola can for instance intersect with the surface edges in 4 locations. This is discussed further in the section on integration, and a integration scheme is presented for those fringe cases as well. Despite this, these 3 cases represent a vast majority of the plume impingement scenarios, and provide the most possibilities to improve integration speeds.

4. Plume Impingement computation

4.1 Pressure function model

Throughout the developments thus far no assumptions on the pressure repartition of the thruster jet are made. The user can therefore input the desired pressure function with the desired behaviors.

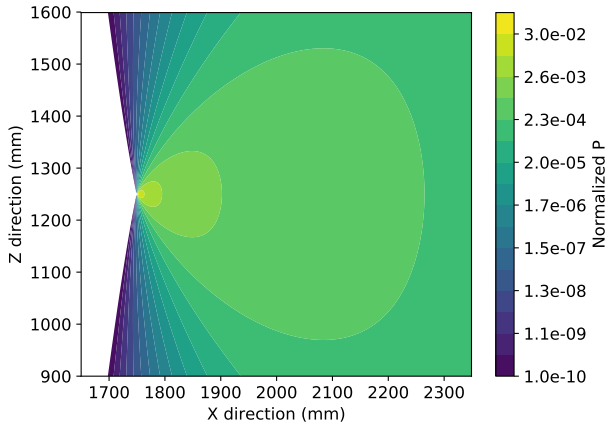

(a) $P_1, i = 3, j = \gamma_0 = 1$

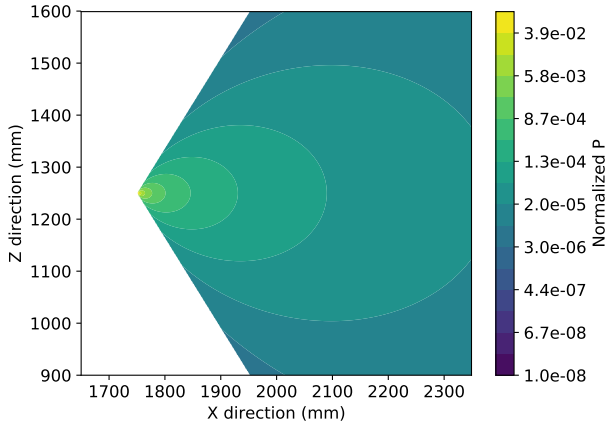

(b) $P_2, i = 3, j = 1.5$

Fig. 7: Different examples of pressure profiles

If a thruster profile is given for a specific mission, example pressure profiles shown in Eqs. (26) and (27) can help fit the data. These functions were developed using basic functions and can be tuned to fit specific data. It is assumed that the pressure output by a thruster depends solely on the distance from the outlet, and the angle from the thruster direction. The vector to the point of interest is noted $\boldsymbol{s}$, and the angle between this vector and the thrust direction $\hat{\boldsymbol{t}}_2$ is noted γ, ie $\gamma = \arccos\left(\hat{\boldsymbol{s}} \cdot \hat{\boldsymbol{t}}_2\right)$. The max thrust of the thruster is $F_{\max}$, and is normalized in these functions in order to output disturbances as percentages of the thrust.

$$P_1(\boldsymbol{s}) = \frac{F_{\max} \cdot e^{\left(\frac{\gamma}{\gamma_0}\right)^i}}{2\pi\left(1-\cos\alpha\right)|\boldsymbol{s}|^j} \tag{26}$$

$$P_2(\boldsymbol{s}) = \frac{F_{\max} \cdot \cos\left(\gamma\right)^i}{2\pi\left(1-\cos\alpha\right)|\boldsymbol{s}|^j} \tag{27}$$

The exponents i, j, and γ_0 are tuning parameters in order to change the shape of the pressure profile. The term on the denominator $2\pi(1-\cos\alpha)$ is the solid angle of the thrust plume cone, giving a measure of how much pressure is lost by the size of the cone half-angle.

Although these pressure functions assume symmetry around the thrust direction, simple modifications could model those imperfections. Furthermore, similar profiles could be also used for temperature profiles when computing heat transfer on impinged surfaces.

The profiles presented in Figure 7 both compare well to the thruster modeling shown in References [10, 11]. Different thrusters in different conditions can yield various plume profiles, and this method allows the user to chose a desired model. It can be noted that shocks have been found to form by the panel, changing the nature of the flow and the resulting pressure, as seen in Reference 12. Although these effects can be modeled, the presented pressure functions yield upper bounds for the disturbance forces and torques that a spacecraft would experience.

4.2 Force and torque integration

In this section the area effected by the thruster plume is integrated to determine the net force and torque imparted onto the spacecraft due to the plume impingement. The hyperbola function of the plume impingement boundary onto the spacecraft surface is determine, as well as the bounds for the surface. This integration nevertheless depends on the cases that were discussed in the previous section and seen in Figure 6.

- Case 1

  With these bounds the minimal and maximal u terms can be found, and a Δu spacial step can be applied along the segment $(u_{\min}, u_{\max})$. These are seen in Figure 8(a)

  For any step $u_k = u_{\min} + k\Delta u$ between the bounds, there is a corresponding segment, $(v_{\min}, v_{\max})$. Where $v_{\min}$ is given by the hyperbola equation, and $v_{\max}$ is given by the panel side equation:

$$v_{\min} = \sqrt{h_2^2\left(\frac{u_k^2}{h_1^2} - 1\right)} \tag{28}$$

$$v_{\max} = \frac{a_{\mathcal{H}}}{b_{\mathcal{H}}}\left(p_u - u_k\right) + p_v \tag{29}$$

- Case 2

  In this case, the $(u_{\min}, u_{\max})$ segment has another intermediate u_{int}. In the case where $u_k \in (u_{\min}, u_{\text{int}})$, both $v_{\min}$ and $v_{\max}$ are given by the panel side equations corresponding to the correct side.

  Once u_{int} has passed, the corresponding segment, $(v_{\min}, v_{\max})$ is defined by the the hyperbola equation and the bounds equations, similarly to the previous case. This is summarized in Figure 8(b).

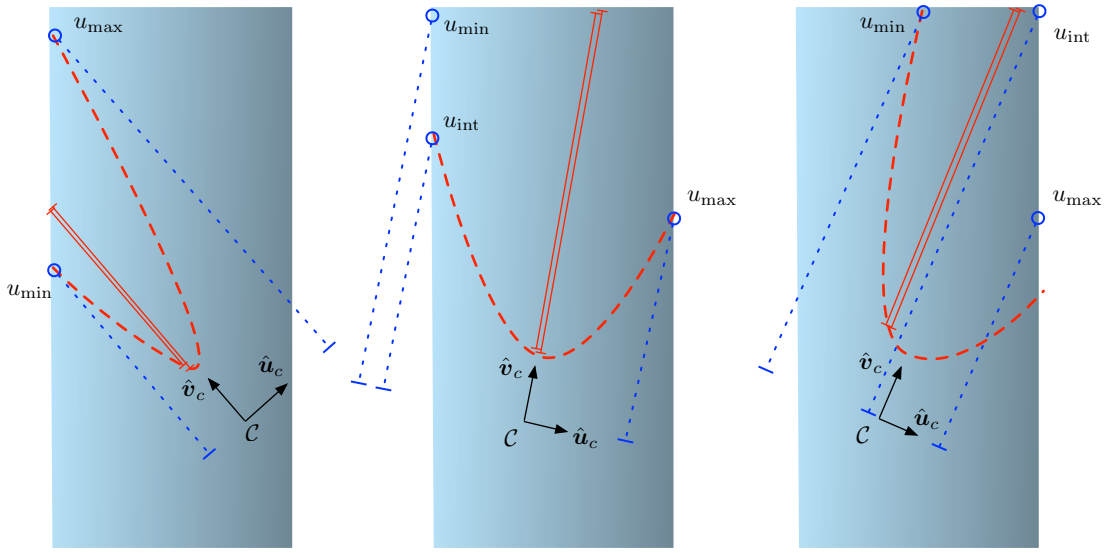

(a) Case 1 (b) Case 2 (c) Case 3

Fig. 8: Examples of impingement scenarios

- Case 3

  Case 3 is equivalent to case 2: there is an intermediate u_{int} at which point the bounds switch between the two different panel side equations. Figure 8(c) displays an example of that scenario.

4.3 Integration in terms of angle

Now that the integration bounds are set for all cases, the summing of the pressure contributions can take place. Due to the general symmetry of the thruster pressure functions, it is of interest to integrate as a function of γ, the angle between the cone axis and the vector pointing to the point at integration. This is done with the knowledge of d, the distance between the thruster and the panel, defined in equation (4). Figure 9(a) shows this integration as seen from above the panel, Figure 9(b) shows the break down of the elements as seen from the side of the panel.

The integration of an infinitesimal surface is considered. It has length $\mathrm{d}v$ perpendicular to the thrust direction, and has a length depending on γ and β. This length is given by:

$$\mathrm{d}v = \frac{s\left(\gamma\right)\mathrm{d}\gamma}{\sin\left(\gamma+\beta\right)} \tag{30}$$

The distance from the thruster to the point of interest using the following relation, where s is the norm of $\boldsymbol{s}$, vector previously defined as the position vector for the integration element relative to the thruster outlet.

$$s(\gamma) = \frac{D}{\sin\left(\gamma+\beta\right)} \tag{31}$$

As defined previously, the pressure is a function of $\boldsymbol{s}$, and therefore can also be parametrized as a function of v and γ assuming that the thruster does not move and due to the symmetry of the pressure function. D is the distance from the thruster to the panel. Therefore we have:

$$P(\boldsymbol{s}) = P(\gamma, v) \tag{32}$$

By integrating the pressure P over u and v, and using Eqs. (30) and (31), the desired formulation is found in Eq. (35)

$$F = \int_{u_{\min}}^{u_{\max}} \int_{v_{\min}(v)}^{v_{\max}(v)} P(\boldsymbol{s})\mathrm{d}u\mathrm{d}v \tag{33}$$

$$= \int_{u_{\min}}^{u_{\max}} \int_{\gamma_{\min}(u)}^{\gamma_{\max}(u)} \frac{P(\gamma,v)s(\gamma)}{\sin\left(\gamma+\beta\right)}\mathrm{d}u\mathrm{d}\gamma \tag{34}$$

$$= \int_{u_{\min}}^{u_{\max}} \int_{\gamma_{\min}(u)}^{\gamma_{\max}(u)} \frac{P(\gamma,v)D}{\sin^2\left(\gamma+\beta\right)}\mathrm{d}u\mathrm{d}\gamma \tag{35}$$

This is a scalar equation. Since the force will be opposite to the panel normal $\hat{\boldsymbol{w}}$, the full equation is given by

$$\boldsymbol{F} = -\left(\int_{u_{\min}}^{u_{\max}} \int_{\gamma_{\min}(u)}^{\gamma_{\max}(u)} \frac{P(\gamma,v)D}{\sin^2\left(\gamma+\beta\right)}\mathrm{d}u\mathrm{d}\gamma\right)\hat{\boldsymbol{w}} \tag{36}$$

Similarly, given the distance to the center of mass B_c of the spacecraft, the associated torques can be evaluated. $\tilde{\boldsymbol{s}}$ is defined to be the vector from the center of mass (B_c) to the point being integrated, while $\boldsymbol{r}_\circ$ is the vector from

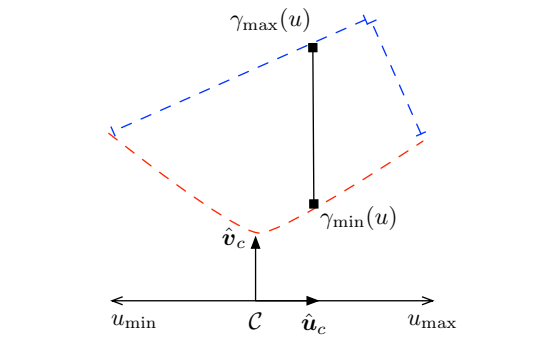

(a) Top view

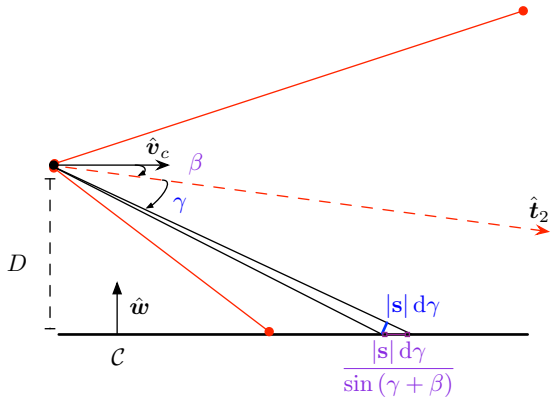

(b) Side view

Fig. 9: Integration schematics

the center of mass to the thruster center. The arm from the center of mass for any point on the panel is therefore

$$\tilde{\boldsymbol{s}} = \boldsymbol{r}_\circ + \boldsymbol{s} \tag{37}$$

Since $\hat{\boldsymbol{w}}$ does not depend on the variables of integration, it is brought into the integral, yielding torque

$$\boldsymbol{T} = \int_{u_{\min}}^{u_{\max}} \int_{\gamma_{\min}(u)}^{\gamma_{\max}(u)} \tilde{\boldsymbol{s}} \times \frac{P(\gamma, v) D}{\sin^2(\gamma+\beta)} \hat{\boldsymbol{w}} \mathrm{d}u \mathrm{d}\gamma \tag{38}$$

This integration scheme is summarized in Figure 9 and provides the expected forces and torques on the spacecraft, given the input pressure function.

4.4 Fringe scenarios

A few assumptions were made in the previous sections. In order to remain comprehensive and robust, solutions are implemented in outlier scenarios. Although this covers the vast majority of the physical outcomes, fringe scenarios can occur. This can be due to unlikely thruster placement, panel placement, and plume geometries, or due to numerical errors. These cases are listed below:

- *Hyperbola not on surface:* In previous analysis, the hyperbola center was on the finite surface, and the hyperbola intersected the finite plane in one of the 3 cases drawn in Figure 6. However the hyperbola center can be off of the surface leading to either no plume impingement or a (nearly) full surface impingement.
- *Inverted hyperbola:* Depending on geometry, and perhaps due to widening the cone in order to achieve a hyperbola, it is possible that the hyperbola be inverted. In this case, it is necessary to integrate under it instead of over it.
- *Non-symmetrical pressure profiles:* For our integration we assumed a symmetry in our pressure profile. A user input pressure function does not necessarily need to have any symmetry.
- *Impingements outside the 3 cases:* As discussed previously, it is possible that other cases of hyperbola intersection be detected. In order to avoid listing subcases all these scenarios are gathered.

All the fringe cases listed above are handled in the same way, and therefore no scenarios are ignored. The integration bypasses the integration bounds, and sums the chosen pressure function over the entire panel. Although there will be loss of speed, the computation will remain physically accurate. This also protects the user from numerical anomalies which could lead to inaccurate force and torque estimates.

5. Results

In order to visualize and validate the work developed in this paper, a plume impingement scenario is simulated. The code was written in the Python programming language.[1] The simulations default parameters for results of Figure 11 are summarized in Table 1.

5.1 Speed vs accuracy

The goal of this method is to simulate thruster plume impingement with high computation speed. In the case of a static spacecraft, this will allow the forces and torques to be computed without slowing down the simulation initialization, and eventually raise flags regarding the thruster and panel placements.

The study also has the vocation of being used in the context of flexible or reconfigurable spacecrafts. Therefore, it is also desired to have a tuning ability for increased speed at the cost of a moderate loss of precision. The following results are given for worst case integration times, in the case of a full surface integration. They therefore provide upper bounds to the numerical evaluation speeds that could be achieved by fully using the method developed in this paper.

Recall the two pressure functions, P_1 defined in Eqs. (26) and P_2 defined in (27). P_1 has a cone greater

[1] https://www.python.org

Table 1: Simulation Parameters

Cases	1	2	3
Panel size $\ell \times L$ (mm)	1000×2000	1000×2000	1000×2000
Panel Center (mm)	${}^{\mathcal{B}}\begin{bmatrix}500 & 1000 & 200\end{bmatrix}^T$	${}^{\mathcal{B}}\begin{bmatrix}500 & 1000 & 200\end{bmatrix}^T$	${}^{\mathcal{B}}\begin{bmatrix}500 & 1000 & 200\end{bmatrix}^T$
Mesh (mm)	$\Delta u = 10$	$\Delta u = 10$	$\Delta u = 10$
Thruster Direction $\hat{\boldsymbol{t}}_2$ (-)	${}^{\mathcal{B}}\begin{bmatrix}\frac{1}{\sqrt{2}} & \frac{1}{\sqrt{2}} & 0\end{bmatrix}^T$	${}^{\mathcal{B}}\begin{bmatrix}\frac{1}{\sqrt{2}} & 0 & 0\end{bmatrix}^T$	${}^{\mathcal{B}}\begin{bmatrix}\frac{1}{\sqrt{2}} & \frac{1}{\sqrt{2}} & 0\end{bmatrix}^T$
Thruster Position (mm)	${}^{\mathcal{B}}\begin{bmatrix}0 & 250 & 200\end{bmatrix}^T$	${}^{\mathcal{B}}\begin{bmatrix}250 & 500 & 200\end{bmatrix}^T$	${}^{\mathcal{B}}\begin{bmatrix}250 & 500 & 200\end{bmatrix}^T$
Cone angle (°)	25	60	60

than $90°$, which leads to smooth continuous pressure profiles. P_2 is a simpler pressure profile with a $60°$ cone. Figure 10(a) shows the convergence of the force and torque values as the mesh size tends towards zero. The curves show slight but minimal oscillations until the mesh size approaches 100 mm. Oscillations start becoming abrupt, and the accuracy of the results is no longer trust-worthy. Indeed, above the 100 mm mark, the mesh becomes coarse in regard to the variations of pressure as seen in Figures 7(a) and 7(b).

Figure 10(b) shows the decrease of the computation time as the mesh size increased. This shows that there is a notable middle-ground between a small loss in accuracy, and a higher computation speed. The mesh sizes between 40 and 60 mm display at most a loss of 1% accuracy relative to the fine meshes, all the while running between 0.1 and 0.05 seconds. It is also noted that even within these fast mesh options, the speed can still be cut in half without too much loss of accuracy, giving knobs for a user to tune.

5.2 Illustration of cases

This section exposes the cases of plume impingement that were discussed in previous parts. In these cases, at least half of the panel is not impinged upon. This not only allows for faster integration, but could also provide local heating information.

Cases 1 through 3 are presented in Figure 11. It is clear from the portion of the surface that is impinged upon, that the integration time could be cut down by using the conical bounding method developed in this paper.

These cases are achieved by displacing the thruster position and direction, and the pressure function cone-angle as seen in Table 1.

5.3 Profile comparison

This section presents the profiles of the pressure and force repartition on the panel. Figure 12 shows simulations which use parameters from Case 2 listed in table 1, with the exception of thruster placement. In Figures 12(a) and 12(b), the thruster is on the edge of the panel: ${}^{\mathcal{B}}\begin{bmatrix}0 & 0 & 200\end{bmatrix}^T$, while in Figures 12(c) and 12(d) the thruster is centered on the panel: ${}^{\mathcal{B}}\begin{bmatrix}0 & 500 & 200\end{bmatrix}^T$.

Figure 12 shows the pressure surface plots on the panel. The panel is visualized in blue, while the surface (both the height in the z direction, and the color) represent the force magnitude for each mesh point. Due to the shape of the pressure function, which decreases with the distance from the thruster and radially from the thruster direction, the surface has a stark peak. Although this is where the majority of the force information is gathered, the torque arm generally increases linearly as the mesh points go farther out on the panel. These grid points therefore remain im-

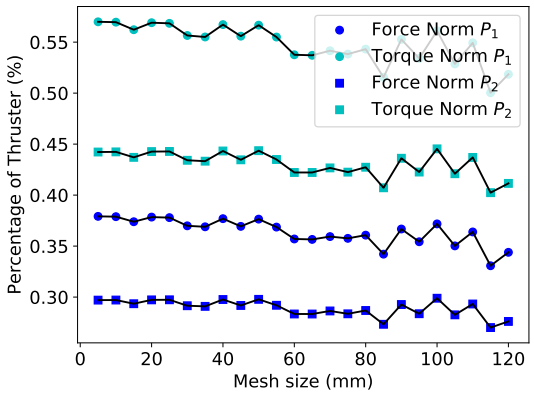

(a) Disturbances as a function of mesh size

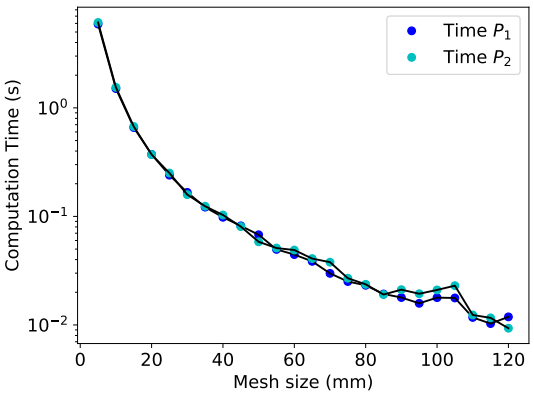

(b) Speed as a function of mesh size

Fig. 10: Code performance

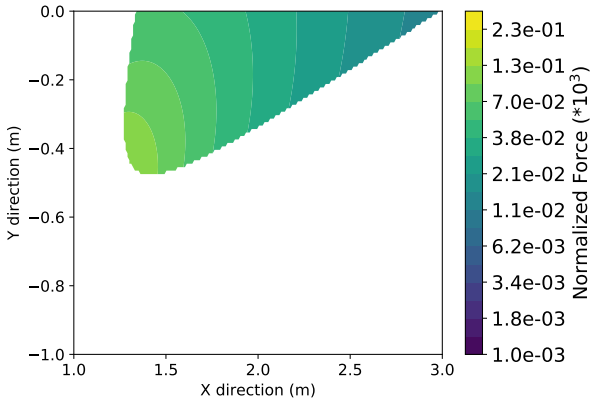

(a) Case 1

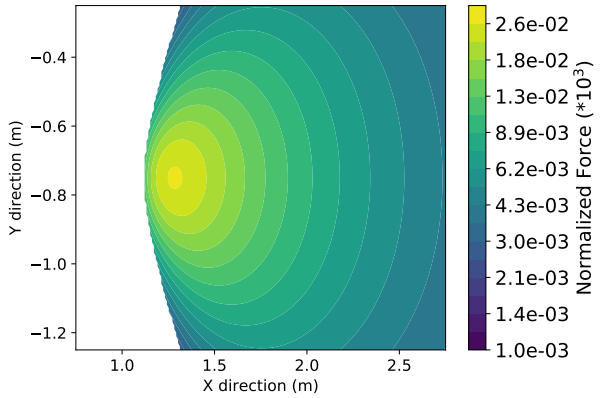

(b) Case 2

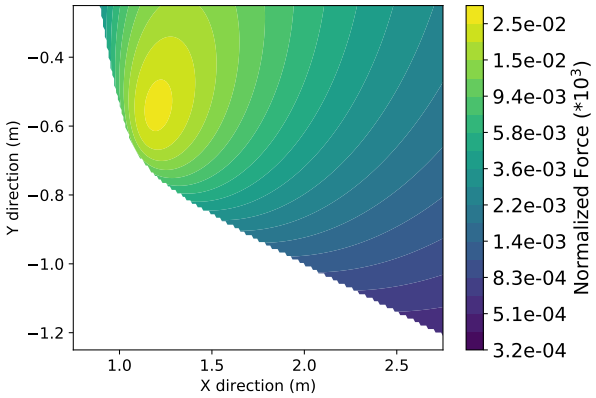

(c) Case 3

Fig. 11: Examples of impingement scenarios with pressure P_2

portant for the torque computation.

Figures 12(a) and 12(b) show the pressure acting upon the surface, with a thruster placed alongside the panel edge. This displays the bell-curve plot that is found in References 3, 12. Furthermore, Figure 12(a) shows a fine mesh grid ($\Delta u = 40$ mm) while Figure 12(b) displays the results of a coarse grid ($\Delta u = 100$ mm). This confirms that at and above $\Delta u = 100$ mm, the mesh grids are too large to capture pressure variations.

Figures 12(c) and 12(d) show the forces acting upon the surface, with a thruster placed on the panel center. This allows the visualization of the force profile for the two different pressure functions given. It is noteworthy that the force values are significantly different, although the disturbance forces and torques are quite similar, as seen in Figure 10(a). This is due to the fact that force is being visualized instead of pressure. Therefore, in the case of P_2 where all the mesh elements are non-zero, the average force values are lower, but more are being added. For the first pressure function P_1, there is less integrated mesh points, but they have a higher value.

Although P_1 in equation (26) does not provide the same level of realism with the sharp pressure cut-off, the profile it yields in Figure 12(c) is a good approximation of the more realistic profile in Figure 12(d).

This allows for a trade off between accuracy and speed: if the user decides to truncated the pressure function and only keep the highly contributing sections of the pressure function, the use of the hyperbola bounds can lead to speed-ups. Indeed, by not integrating large sections of the panel, the computation time can be cut down 2 or 3 fold, depending on the percentage of the panel that is covered with plume.

The pressure profile shapes seen in the plots of Figure 12, seen on the edge of the surfaces compare well in shape and size with References 12–14

6. Conclusions

The methods described throughout this paper display promise for a fast, automated plume impingement model to evaluate the disturbance forces and torques. Even by implementing worst-case, full panel integrations, a useful range of parameters allowing for a fast and modular plume impingement test are shown. Results compare well

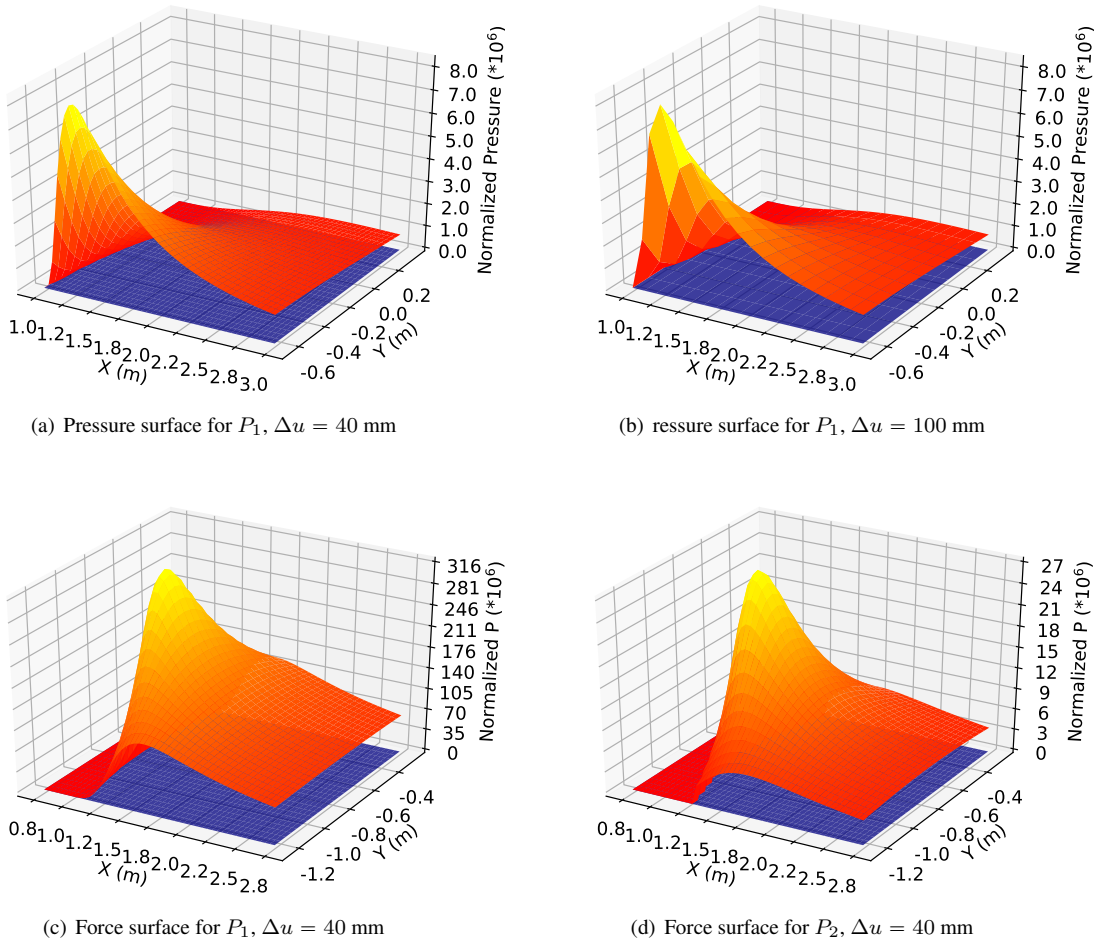

(a) Pressure surface for P_1, $\Delta u = 40$ mm

(b) ressure surface for P_1, $\Delta u = 100$ mm

(c) Force surface for P_1, $\Delta u = 40$ mm

(d) Force surface for P_2, $\Delta u = 40$ mm

Fig. 12: Force and pressure visualizations

to other thrust impingement models, all the while bypassing the need for computationally intensive operations.

Future research could add a heat exchange model in order to simulate panel heating. The hyperbola formulation allows for local heating estimates, and the array of possible pressure functions could also be used for defining temperature profiles. In the case of symmetric plume modeling, there is still some computational speed that could be gained. Developing a more analytical integration by using the constant pressure profiles along hyperbolas imbedded in the within the bounding hyperbola is a potential next step.

REFERENCES

[1] Keith C Kannenberg. Three dimensional monte carlo simulations of plume impingement. *American Institutefo Aeronautics and Astronautics, Inc.*, (AIAA 98-2755):99–112, 1998.

[2] Zhang Jianhua. Numerical and experimental study of plume impingement effects. Rarefied Gas Dynamics: 22nd International Symposium, 2006.

[3] Xi Chen. Impact on an inclined flat plate exposed to a rarefied plasma plume. *JOURNAL OF SPACECRAFT AND ROCKETS*, 49(4), July-August 2012.

[4] Forrest E. Lumpkin. A cfd/dsmc analysis of plumes and plume impingement during shuttle/mir docking. *30th AIAA Thermophysics Conference*, pages 593–598, June 1995.

[5] C. B. Madden. Space station plume impingement heating. 1994.

[6] Wm. C.Rochelle. Plume impingement heating to international space station (iss). Number AlAA 95-2132, June 1995.

[7] S.A. Parvez. Satellite disturbance due to thruster plume impingement on solar array. *American Institute of Aeronautics and Astronautics, Inc*, 1994.

[8] Hanspeter Schaub and John L. Junkins. *Analytical Mechanics of Space Systems*. AIAA Education Series, Reston, VA, 3rd edition, 2014.

[9] G. T. Korn. *A Mathematical Handbook for Scientists and Engineers: Definitions, Theorems, and Formulas for Reference and Review*. Dover, second edition edition, 2000.

[10] Iain D. Boyd. Review of hall thruster plume modeling. *Journal of Spacecraft and Rockets*, 38(3):381–387, 2017/09/02 2001.

[11] Ioannis Mikellides, Lee Johnson, Ira Katz, and M. Mandell. *A High Power Ion Thruster Plume Model*. American Institute of Aeronautics and Astronautics, 2017/09/02 2004.

[12] George Dettleff. Plume flow and plume impingement in space technology. *Prog. Aerospace Sci.*, 28:1–71, 1991.

[13] H Legge. Plume impingement forces on inclined flat plates. *Rarefied gas dynamics: proceedings of the 17th international symposium*, 7(1):955–962, July 1991.

[14] K. Khasawneh. Rarefied compressible two-dimensional jet plume impingement on a flat plate. 49th AIAA Aerospace Sciences Meeting, 2011.